



Evaluation of performance of CMIP5 models in simulating the North Pacific Oscillation and El Niño Modoki

Xin Wang^{1,2} · Mengyan Chen^{1,3} · Chunzai Wang¹ · Sang-Wook Yeh⁴ · Wei Tan^{2,5}

Received: 16 October 2017 / Accepted: 1 April 2018 / Published online: 4 April 2018
© Springer-Verlag GmbH Germany, part of Springer Nature 2018

Abstract

Previous observational studies have documented that the occurrence frequency of El Niño Modoki is closely linked to the North Pacific Oscillation (NPO). The present paper evaluates the relationships between the frequency of El Niño Modoki and the NPO in the historical runs of the Coupled Model Intercomparison Project Phase 5 (CMIP5) and examines the related physical processes. It is found that six of 25 CMIP5 models can reproduce both the spatial patterns of the NPO and El Niño Modoki. Four of these six models exhibit good performance in simulating the positive correlation between the NPO index and the frequency of El Niño Modoki. The analyses further show that the key physical processes determining the relationships between the NPO and the frequency of El Niño Modoki are the intensity of wind-evaporation-SST (WES) feedback in the subtropical northeastern North Pacific. This study enhances the understanding of the connections between the North Pacific mid-latitude climate system and El Niño Modoki, and has an important implication for the change of El Niño Modoki under global warming. If global warming favors to produce an oceanic and atmospheric pattern similar to the positive phase of the NPO in the North Pacific, more El Niño Modoki events will occur in the tropical Pacific with the assistance of the WES feedback processes.

Keywords El Niño Modoki · North Pacific Oscillation · CMIP5 climate models

1 Introduction

Based on their different locations of the maximum sea surface temperature (SST) anomalies, two types of El Niño events, i.e., canonical El Niño and El Niño Modoki events,

have been emphasized in recent years (e.g., Larkin and Harrison 2005; Yu and Kao 2007; Ashok et al. 2007; Kao and Yu 2009; Kug et al. 2009). The latter is also referred to as the Date Line El Niño (Larkin and Harrison 2005), central Pacific El Niño (Yu and Kao 2007), or warm pool El Niño (Kug et al. 2009). Although anomalous SST warm centers locate in the central tropical Pacific, the distributions of the SST anomalies of El Niño Modoki and central Pacific El Niño show differences in the eastern tropical Pacific. El Niño Modoki shows a zonal tripole structure with warm SST anomalies in the central equatorial Pacific flanked by cold SST anomalies in the eastern and western Pacific (Ashok et al. 2007). However, warm SST anomalies may appear in the eastern tropical Pacific for central Pacific El Niño (Yu and Kao 2007). Wang et al. (2016) provided a detailed overview of ENSO including different types of El Niño events.

A great number of studies have demonstrated that El Niño Modoki and canonical El Niño affect global weather and climate differently (e.g., Weng et al. 2007; Kim et al. 2009; Taschetto and England 2009; Mo 2010; Wang et al. 2014; Yuan and Yang 2012; Yu et al. 2012b; Liu et al. 2014; Wang and Wang 2013, 2014; Tan et al. 2016). Yuan and

✉ Xin Wang
wangxin@scsio.ac.cn

- ¹ State Key Laboratory of Tropical Oceanography, South China Sea Institute of Oceanology, Chinese Academy of Sciences, 164 West Xingang Rd., Guangzhou 510301, People's Republic of China
- ² Laboratory for Regional Oceanography and Numerical Modeling, Qingdao National Laboratory for Marine Science and Technology, Qingdao 266237, People's Republic of China
- ³ University of Chinese Academy of Sciences, Beijing 100049, People's Republic of China
- ⁴ Department of Marine Sciences and Convergent Technology, Hanyang University, Ansan, South Korea
- ⁵ First Institute of Oceanography, State Oceanic Administration, Qingdao 266061, People's Republic of China

Yang (2012) found that during developing summer, El Niño Modoki exerts a stronger impact on East Asian climate than canonical El Niño. This finding is consistent with the result proposed by Weng et al. (2007). In contrast, the impact of canonical El Niño on East Asian climate is more significant than the influence of El Niño Modoki during decaying summer due to the long-lasting anomalous warming over the tropical Indian Ocean accompanying with canonical El Niño (Yuan and Yang 2012). North American climate is also significantly related to two types of El Niño. Mo (2010) and Yu et al. (2012b) found that two types of El Niño exert different impacts on American winter temperature. In contrast to canonical El Niño, El Niño Modoki events lead to more frequent and increasing landfall potential of tropical cyclones along Central America and the Gulf of Mexico coast (Kim et al. 2009). Yu et al. (2017) summarized and compared the climate impacts of El Niño Modoki and canonical El Niño.

However, there is no consensus on the mechanisms of how El Niño Modoki occurs. Kug et al. (2009) indicated that the zonal advective feedback plays a crucial role in the SST evolution of El Niño Modoki. According to the analysis of El Niño in CMIP3 model future climate projections, Yeh et al. (2009) suggested that global warming could lead to a flattening or shoaling of the equatorial thermocline in the equatorial Pacific, which results in more frequent El Niño Modoki occurrence. Some researchers suggested that there is a connection between the tropical SST and mid-latitude atmosphere variability (Vimont et al. 2003a, b; Jin and Kirtman 2009; Di Lorenzo et al. 2010; Yu et al. 2010, 2012a; Yu and Kim 2011; Deser et al. 2012; Furtado et al. 2012; Anderson et al. 2013b; Park et al. 2013; Ding et al. 2015a, b, 2017; Yeh et al. 2015; Ma et al. 2017). Vimont et al. (2001) indicated that previous winter mid-latitude atmospheric variability could affect the following summer equatorial wind stress anomalies via the seasonal footprinting mechanism. This, however, is not the primary ENSO mechanism but rather a particularly effective component of the stochastic forcing of ENSO (Vimont et al. 2003a, b). Furthermore, several studies indicated that the variability of El Niño Modoki is greatly associated with the North Pacific Oscillation (NPO) (Yu and Kim 2011; Yu et al. 2012a; Furtado et al. 2012; Yeh et al. 2015). The NPO is characterized by a meridional dipole in sea level pressure (SLP), and usually defined as the second mode of empirical orthogonal function (EOF) of SLP in the North Pacific (Walker and Bliss 1932; Rogers 1981). In addition to global warming (Yeh et al. 2009), the variations of the NPO can result in the increasing occurrence of El Niño Modoki (Yu et al. 2012a; Yeh et al. 2015). Yu et al. (2012a) pointed out that the NPO could excite large SST variability in the tropical Pacific after 1990, which leads to a strengthening of the Hadley circulation and thus the increasing occurrence of El Niño Modoki after 1990. Yeh et al. (2015) found that the wind-evaporation-SST (WES) feedback process in the

subtropical northeastern Pacific induced by the NPO-like atmospheric circulations shifts southward, and thus favors the generation of the westerly wind anomaly close to the central equatorial Pacific, leading to the frequent occurrence of El Niño Modoki after 1990. Other studies also pointed out that the occurrence of El Niño Modoki is related to the Atlantic remote forcing (e.g., Ham et al. 2013; Ding et al. 2016).

Based on the observed results, previous studies show that the occurrences of El Niño Modoki are closely associated with the NPO. However, the performance of the current state-of-the-art models in simulating the connections between El Niño Modoki and the North Pacific atmospheric circulation is not yet clear. The purpose of this paper is to evaluate the simulated relationships between the NPO and the frequency of El Niño Modoki in Coupled Model Intercomparison Project Phase 5 (CMIP5) climate models. By comparing the relationships of the NPO with the occurrences of El Niño Modoki and related physical dynamic processes in coupled models, it is helpful to further understand the subtropical-tropical interactions and improve the simulation ability of models. The paper is organized as follows. In Sect. 2, the data sets and methodology used in the study are introduced. Section 3 assesses the abilities of CMIP5 models in simulating the NPO and El Niño Modoki. Section 4 evaluates the relationships between the NPO and the frequency of El Niño Modoki in CMIP5 models, and examines the dynamical processes linking the NPO and El Niño Modoki occurrences. Finally, summary and discussion are presented in Sect. 5.

2 Data sets and method

The monthly SST from the Hadley Centre Sea Ice and SST dataset (HadISST) with a $1.0^\circ \times 1.0^\circ$ resolution is used (Rayner et al. 2003). The monthly SLP and surface wind with a resolution of $2.5^\circ \times 2.5^\circ$ are obtained from the National Centers for Environmental Prediction/National Center for Atmospheric Research (NCEP/NCAR) Reanalysis 1 (Kalnay et al. 1996). The 25 CMIP5 model outputs from the historical run are used in this study (Table 1). It is noted that the simulations of HadGEM2-CC and HadGEM2-ES end in November, 2005. Therefore, we analyze all model outputs and observations spanning from 1950 to 2004.

The data from observations and models are detrended and the climatological seasonal cycle is removed. Correlation analysis, EOF analysis and combined EOF (CEOF) analysis are applied in this study. When calculating the significant test of pattern correlations between the models and observations, the effective number of degrees of freedom N^* is identified as (Bretherton et al. 1999)

$$N^* = N \frac{1 - r_x r_y}{1 + r_x r_y}$$

Table 1 Description of models obtained from the CMIP5 archives

Number	CMIP5 ID	Surface wind and SLP resolution (lon × lat)	SST resolution (lon × lat)	Available period
1	ACCESS1-0	1.88° × 1.25°	1.00° × (0.33°–1.00°)	185,001–200,512
2	bcc-csm1-1	2.81° × 2.75°	1.00° × (0.33°–1.00°)	185,001–200,512
3	CanESM2	2.81° × 2.79°	1.41° × 0.93°	185,001–200,512
4	CMCC-CESM	3.75° × 3.71°	1.99° × 1.22°	185,001–200,512
5	CNRM-CM5	1.41° × 1.41°	1.00° × 0.33°	185,001–200,512
6	CSIRO-Mk3.6.0	1.88° × 1.87°	1.88° × 0.93°	185,001–200,512
7	FGOALS-s2	2.81° × 1.66°	1.00° × (0.5°–1.00°)	185,001–200,512
8	GFDL-ESM2G	2.50° × 2.00°	1.00° × 0.86°	186,101–200,512
9	GFDL-ESM2M	2.50° × 2.00°	1.00° × 0.90°	186,101–200,512
10	GISS-E2-H	2.50° × 2.00°	2.50° × 2.00°	185,001–200,512
11	GISS-E2-H-CC	2.50° × 2.00°	2.50° × 2.00°	185,001–201,012
12	GISS-E2-R	2.50° × 2.00°	2.50° × 2.00°	185,001–200,512
13	GISS-E2-R-CC	2.50° × 2.00°	2.50° × 2.00°	185,001–201,012
14	HadCM3	3.75° × 2.47°	1.25° × 1.25°	185,001–200,512
15	HadGEM2-CC	1.88° × 1.25°	1.00° × (0.30°–1.00°)	185,912–200,511
16	HadGEM2-ES	1.88° × 1.25°	1.00° × (0.30°–1.00°)	185,912–200,511
17	inmcm4	2.00° × 1.50°	1.00° × 0.50°	185,001–200,512
18	IPSL-CM5A-LR	3.75° × 1.88°	2.00° × (0.50°–2.00°)	185,001–200,512
19	IPSL-CM5A-MR	2.50° × 1.25°	2.00° × (0.50°–2.00°)	185,012–200,512
20	IPSL-CM5B-LR	3.75° × 1.88°	2.00° × (0.50°–2.00°)	185,001–200,512
21	MIROC5	1.41° × 1.41°	1.4° × (0.50°–1.40°)	185,001–200,512
22	MPI-ESM-LR	1.88° × 1.87°	1.40° × 0.82°	185,001–200,512
23	MPI-ESM-MR	1.88° × 1.87°	1.40° × 0.82°	185,001–200,512
24	MPI-ESM-P	1.88° × 1.87°	1.40° × 0.82°	185,001–200,512
25	MRI-CGCM3	1.13° × 1.12°	1.00° × 0.50°	185,001–200,512

where N represents the number of available sample, r_x and r_y are the lag 1 autocorrelations of variables x and y , respectively.

3 Definitions of the NPO and El Niño Modoki in CMIP5

To evaluate the relationships between the NPO and the frequency of El Niño Modoki in CMIP5 models, we first assess the abilities of models in simulating the NPO and El Niño Modoki. Only models reproducing both the NPO and El Niño Modoki are used to further examine their performances of the connections of the NPO with El Niño Modoki in next section.

Usually, the NPO is identified by the second EOF mode of SLP anomalies in the North Pacific (Rogers 1981). In this study, an EOF analysis of the March–April–May (MAM) averaged SLP anomalies in the North Pacific (20°N–60°N, 120°E–120°W) is applied in observations and CMIP5 model outputs, and the corresponding second leading modes (EOF2) are shown in Fig. 1. From observations, the signals in the subtropical Pacific and the higher-latitude Pacific are

out-of-phase, and such pattern accounts for 20.1% of the total variance (Fig. 1a). The negative and positive centers are located around (35°N, 150°W) and (60°N, 150°W), respectively, which is similar to the results of others (Yu et al. 2012a, b; Yeh et al. 2015). Most of the models, except for MRI-CGCM3, can well reproduce the meridional dipole modes of the EOF of the SLP anomalies in the North Pacific with significantly spatial correlation coefficients. Although most of the models can simulate the meridional dipole of the SLP, the meridional dipole in many models show longitudinal shift compared with the observations (Fig. 1). For example, the locations of the maximum and minimum SLP anomaly centers in several models (i.e., CSIRO-Mk3.6.0, GFDL-ESM2G, GISS-E2-H, GISS-E2-R, IPSL-CM5A-LR, IPSL-CM5A-MR, inmcm4, and MPI-ESM-P) are different from the observed centers. Different from the observation and the other models, the second leading EOF mode of SLP anomalies in MRI-CGCM3 shows a zonal dipole pattern in the North Pacific, which is poorly related to the observation (spatial correlation coefficient is -0.2). We also examine the third mode (EOF3) in the MRI-CGCM3, which shows a zonal tripole structure (figure not shown). It is suggested that the MRI-CGCM3 cannot capture the feature of the NPO.

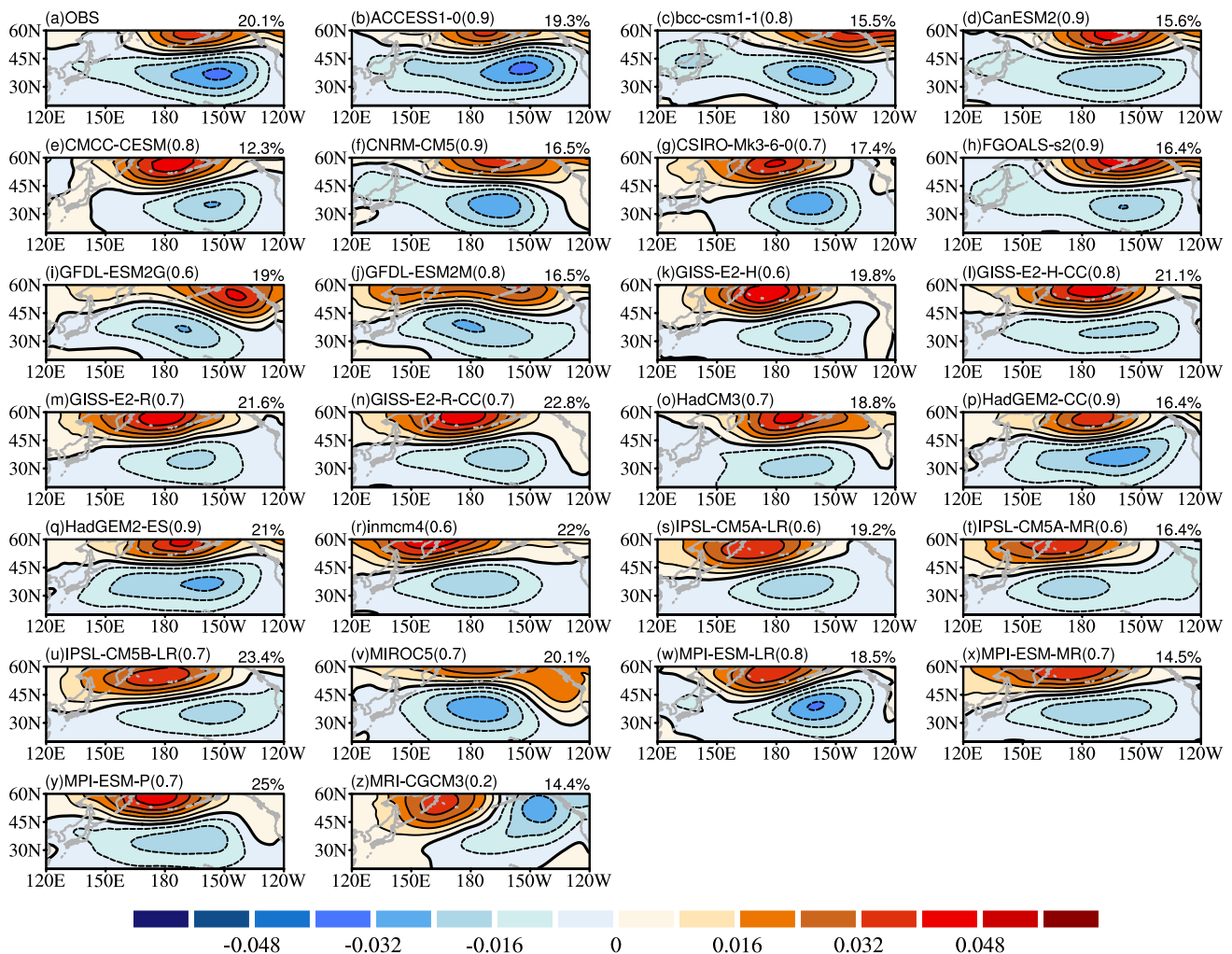


Fig. 1 Spatial patterns of the second EOF mode of the MAM-averaged SLP anomalies over the North Pacific (20°N – 60°N , 120°E – 120°W) calculated from observation (**a**) and 25 CMIP5 models (**b**–**z**). The numbers at the upper right of each panel indicate the percentage of variance explained by each model's second EOF mode. Pattern correlation coefficients between each model and observation

are shown in parentheses (*the statistical significance at the 95% confidence level). The EOF2 modes in ACCESS1-0, bcc-csm1-1, CanESM2, CMCC-CESM, CNRM-CM5, CSIRO-MK3-6-0, GFDL-ESM2G, GISS-E2-R, HadGEM2-CC, IPSL-CM5A-MR, MIROC5, MPI-ESM-LR, MPI-ESM-P and MRI-CGCM3 are multiplied by -1

Due to its poor performance in simulating the NPO, the output of MRI-CGCM3 is not used in the following section. Here, the normalized time series of the second principal component (PC2) in the observation and models are defined as the NPO index (Park et al. 2013).

Several methods are proposed to identify El Niño Modoki (e.g., Ashok et al. 2007; Kug et al. 2009; Yeh et al. 2009; Ren and Jin 2011; Kim and Yu 2012; Taschetto et al. 2014). The performances of CMIP3 and CMIP5 (Coupled Model Intercomparison Project Phases 3 and 5) models in simulating the two types of El Niño have been evaluated (Yu and Kim 2010; Ma and Yu 2014; Taschetto et al. 2014; Xu et al. 2016). Yu and Kim (2010) and Ma and Yu (2014) adopted a combined regression-EOF analysis to identify two types of El Niño in CMIP3 and CMIP5 models. To obtain the

SST anomaly pattern for the canonical El Niño (El Niño Modoki), they first remove the tropical SST anomalies that are regressed with the Niño4 SST (Niño 1+2) index and then apply the EOF analysis to the residual SST anomalies. Taschetto et al. (2014) distinguished the two types of El Niño events in the following way: an event is regarded as a canonical El Niño (El Niño Modoki) when the Niño3 index is greater (lower) than Niño4 index, and the Niño3 (Niño4) index is above one standard deviation. They suggested that most of models capture the observed peak in ENSO amplitude around December and CMIP5 models generally reproduce the duration of El Niño Modoki through analyzing 34 CMIP5 models. Xu et al. (2016) classified El Niño events in CMIP5 model simulations by EOF analysis on the filtered monthly mean SST and they suggested that CMIP5 models

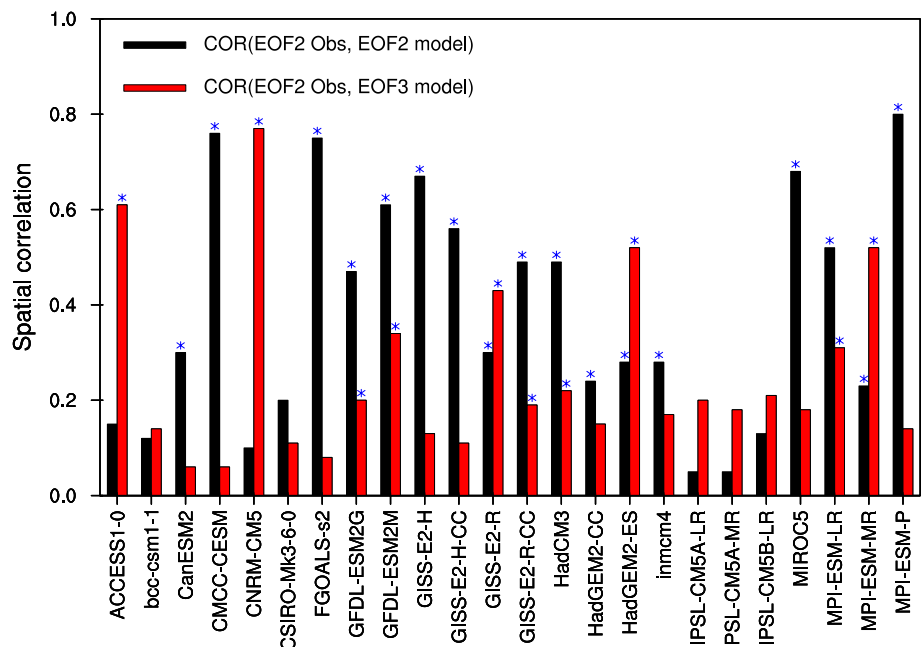
are more capable in reproducing the observed canonical El Niño, but less so for El Niño Modoki. The performances of models in simulating El Niño Modoki are associated with the method applied to define and identify El Niño Modoki. To validate the performances of CMIP5 models in simulating El Niño Modoki, two of these methods are adopted in the study.

In the study, an EOF analysis of the DJF-averaged SST anomalies over the tropical Pacific (30°S–30°N, 120°E–70°W) is performed in the observation and the historical runs from 24 CMIP5 models. As Xu et al. (2016) found, the characteristics of El Niño Modoki can be described by the EOF2 or EOF3 mode in models. The pattern correlation coefficients of the observed EOF2 with the simulated EOF2 and EOF3 are checked in Fig. 2. The pattern correlation coefficients of the observed EOF2 with the EOF2 in nine models (CanESM2, CMCC-CESM, FGOALS-s2, GISS-E2-H, GISS-E2-H-CC, HadGEM2-CC, inmcm4, MIROC5 and MPI-ESM-P) are exceeding 95% significance, while the pattern correlation coefficients between the EOF3 modes in these models and the observation EOF2 are not. In ACCESS1-0 and CNRM-CM5, the simulated EOF3 patterns are significantly correlated with the observed EOF2, but their simulated EOF2 patterns do not. Therefore, the normalized time series of the 2nd and 3rd principal component (PC2 and PC3) in nine models (CanESM2, CMCC-CESM, FGOALS-s2, GISS-E2-H, GISS-E2-H-CC, HadGEM2-CC, inmcm4, MIROC5 and MPI-ESM-P) and two models (ACCESS1-0 and CNRM-CM5) are used as the El Niño Modoki indices, respectively. The simulated EOF2 and EOF3 patterns in eight models (GFDL-ESM2G, GFDL-ESM2M, GISS-E2-R, GISS-E2-R-CC, HadCM3,

HadGEM2-ES, MPI-ESM-LR and MPI-ESM-MR) are both significantly correlated with the observed EOF2 pattern. Here, El Niño Modoki-like mode in the eight models is defined by the EOF pattern and their pattern correlation coefficient with the observed EOF2 is higher. That is to say, the simulated EOF2 (EOF3) is defined as El Niño Modoki mode if the pattern correlation coefficient of the observed EOF2 is higher than that with EOF3 (EOF2). In a summary, there are 19 models in which the EOF2/EOF3 patterns are similar to the observed EOF2 pattern, indicating that the feature of El Niño Modoki with the tripole pattern of SST variability is well captured in these models. The corresponding 2nd principal component (PC2) in 14 models and PC3 in 5 models are normalized and used as El Niño Modoki indices for models. Therefore, an El Niño Modoki event is defined when the normalized PC2/PC3 is equal to or greater than 0.7σ , which is named as the method 1-El Niño Modoki (M1-El Niño Modoki) in present study. However, in the other five models (bcc-csm1-1, CSIRO-Mk3-6-0., IPSL-CM5A-LR, IPSL-CM5A-MR, and IPSL-CM5B-LR), the pattern correlations of the observed EOF2 with the simulated EOF2 and EOF3 are rather low, indicating that they fail to reproduce the warm SST anomalies in the central tropical Pacific. These five models are therefore not analyzed further.

El Niño Modoki events identified by the different methods can show some differences both from the observation (Yu and Kim 2013) and model outputs (Yu and Kim 2010; Taschetto et al. 2014; Xu et al. 2016). To confirm the above identified M1-El Niño Modoki in models, the definition of El Niño Modoki used by Kug et al. (2009), Yeh et al. (2009) and Taschetto et al. (2014) is also applied. Here, an El Niño Modoki event is defined by the DJF-averaged Niño4 index

Fig. 2 Spatial correlation coefficients between the observed second leading EOF (EOF2) and simulated EOF2 (black bar), and EOF3 (red bar) from historical runs of each of the 24 CMIP5 climate models. The blue asterisks indicate the statistical significance at the 95% confidence level



being equal to or greater than 0.7σ , and the value of the winter Niño4 index being greater than winter Niño3 index, which is named as the Method 2-El Niño Modoki (M2-El Niño Modoki) in present study. To compare M1-El Niño Modoki and M2-El Niño Modoki, the composites of SST anomalies during DJF in the tropical Pacific (30°S – 30°N , 120°E – 70°W) for the M1-El Niño Modoki and M2-El Niño Modoki are firstly calculated in the observation and models, respectively. The pattern correlation coefficients between the composited SST anomaly patterns for M1-El Niño Modoki and M2-El Niño Modoki are calculated and shown in Fig. 3. In the observation, the pattern correlation coefficient between the M1-El Niño Modoki and M2-El Niño Modoki SST anomalies is as high as about 0.56. Six models, including CanESM2, FGOALS-s2, GFDL-ESM2M, GISS-E2-R-CC, HadCM3, and MIROC5, exhibit significantly positive pattern correlation coefficients as well as the observation, indicating that the El Niño Modoki events identified by the two definitions are similar in these model outputs. Therefore, only these six models are used to analyze the NPO-El Niño Modoki relationships. The composites of SST anomalies in the observation and these selected six CMIP5 models (CanESM2, FGOALS-s2, GFDL-ESM2M, GISS-E2-R-CC, HadCM3, and MIROC5) by using two methods to define El Niño Modoki is shown in Fig. 4. It could be seen that

although the SST anomalies show some differences in terms of spatial pattern and intensity in observation and model simulations, strongly warm SST anomalies are seen in the central tropical Pacific and northern subtropical Pacific during El Niño Modoki identified by two methods, except for GISS-E2-R-CC (Fig. 4). The warm SST anomalies of M2-El Niño Modoki in GISS-E2-R-CC in the northern subtropical Pacific are rather weaker than others. It is suggested that most models could reproduce the spatial patterns of warm SST anomalies in the central tropical Pacific and northern subtropical Pacific of El Niño Modoki to some degrees.

4 Performance of linkage between the NPO and El Niño Modoki in CMIP5

4.1 The simulated NPO-El Niño Modoki relationships

Yeh et al. (2015) suggested that the frequent occurrence of El Niño Modoki after the 1990s is closely associated with NPO variability because the WES feedback process in the subtropical northeastern Pacific associated with the NPO becomes more effective to excite El Niño Modoki. This section mainly evaluates performance of the relationships

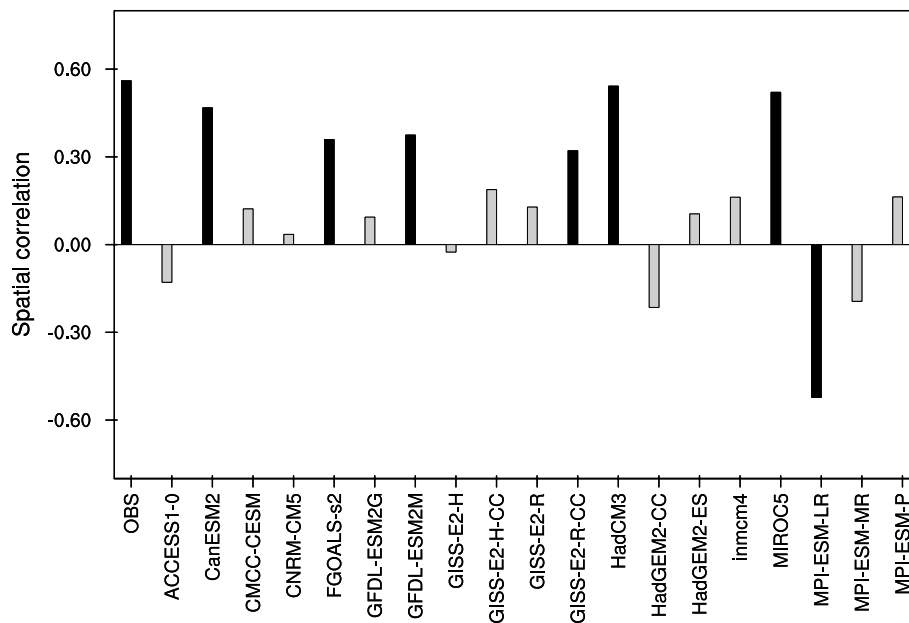
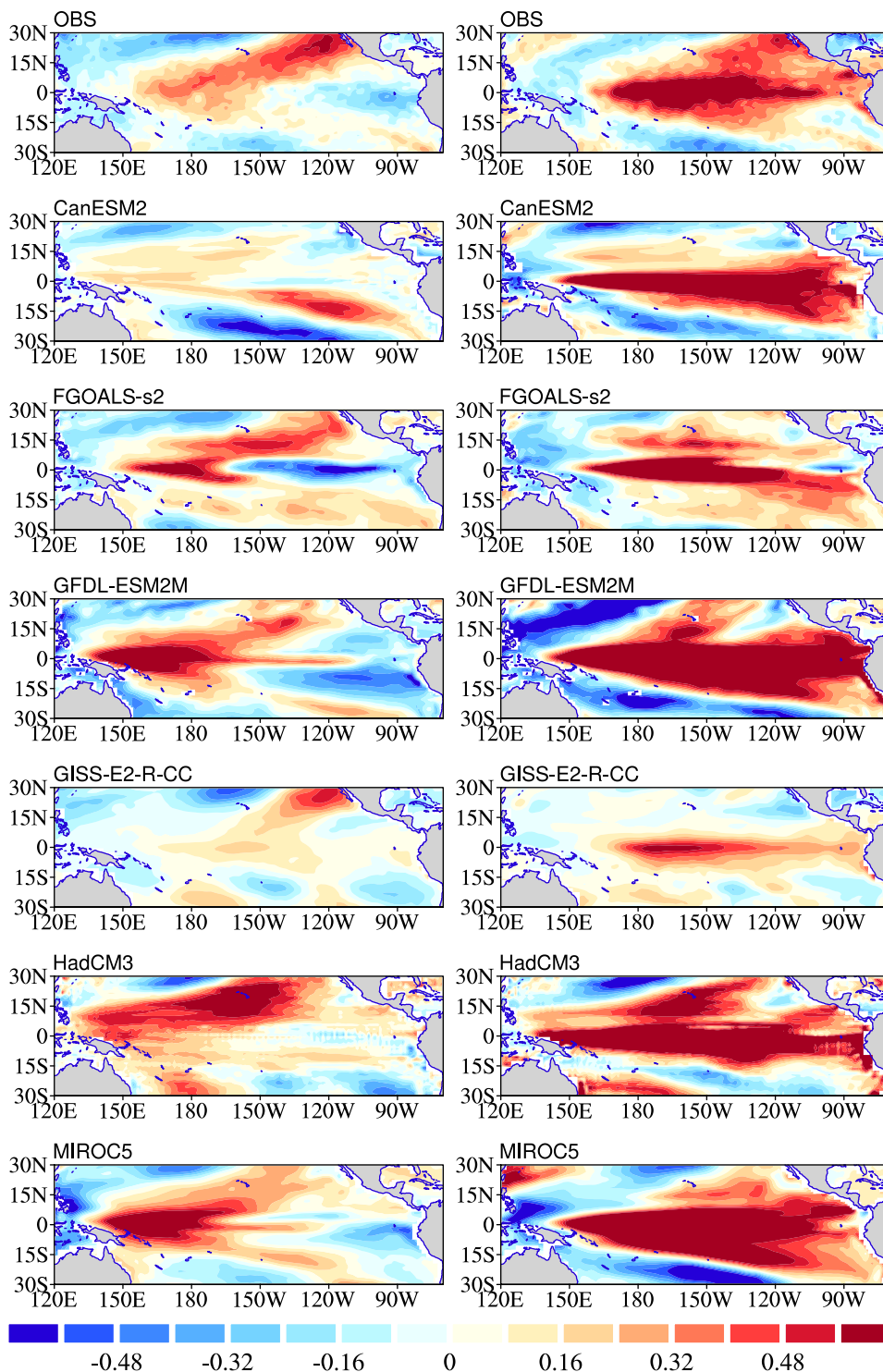


Fig. 3 Pattern correlation coefficients between composites of DJF SST anomalies in the tropical Pacific (30°S – 30°N , 120°E – 70°W) for the M1-El Niño Modoki and M2-El Niño Modoki in the observation and models. M1-El Niño Modoki is defined if the normalized PC2 (CanESM2, CMCC-CESM, FGOALS-s2, GFDL-ESM2G, GFDL-ESM2M, GISS-E2-H, GISS-E2-H-CC, GISS-E2-R-CC, HadCM3, HadGEM2-CC, inmcm4, MIROC5, MPI-ESM-LR, and MPI-ESM-P) or PC3 (ACCESS1-0, CNRM-CM5, GISS-E2-R, HadGEM2-ES and

MPI-ESM-MR) of the DJF-averaged SST anomalies over the tropical Pacific are equal to or greater than 0.7σ . M2-El Niño Modoki event is selected when the DJF-averaged Niño4 index is equal to or greater than 0.7σ and the value of the winter Niño4 index is greater than winter Niño3 index. Black (gray) bars indicate the correlation coefficients exceeding (not exceeding) 95% statistical significance level based on a Student's t test

Fig. 4 Composites of SST anomalies ($^{\circ}\text{C}$) during the DJF for M1-El Niño Modoki (left panel) and M2-El Niño Modoki (right panel) in the observation and six CMIP5 models. M1-El Niño Modoki is defined if the normalized PC2 (CanESM2, CMCC-CESM, FGOALS-s2, GFDL-ESM2G, GFDL-ESM2M, GISS-E2-H, GISS-E2-H-CC, GISS-E2-R-CC, HadCM3, HadGEM2-CC, Inmcm4, MIROC5, MPI-ESM-LR, and MPI-ESM-P) or PC3 (ACCESS1-0, CNRM-CM5, GISS-E2-R, HadGEM2-ES and MPI-ESM-MR) of the DJF-averaged SST anomalies over the tropical Pacific are equal to or greater than 0.7σ . M2-El Niño Modoki event is selected when the DJF-averaged Niño4 index is equal to or greater than 0.7σ and the value of the winter Niño4 index is greater than winter Niño3 index



between the frequency of El Niño Modoki and the NPO in selected six CMIP5 models, and examines what the simulated biases result from. Here, an El Niño Modoki event is referred to the M1-El Niño Modoki. In this study, the frequency of El Niño Modoki means the number of El Niño Modoki in sliding 21 years. Figure 5 shows the correlation coefficients between 21-year running mean NPO indices and

the frequency of El Niño Modoki in the observation and models. In the observation, a significantly positive correlation between the frequency of El Niño Modoki and the NPO is seen as high as 0.45, indicating that the positive phase of the NPO is in favor of the frequent occurrence of El Niño Modoki. It is in agreement with previous studies (Yu et al. 2012a; Yeh et al. 2015). A positive phase of the

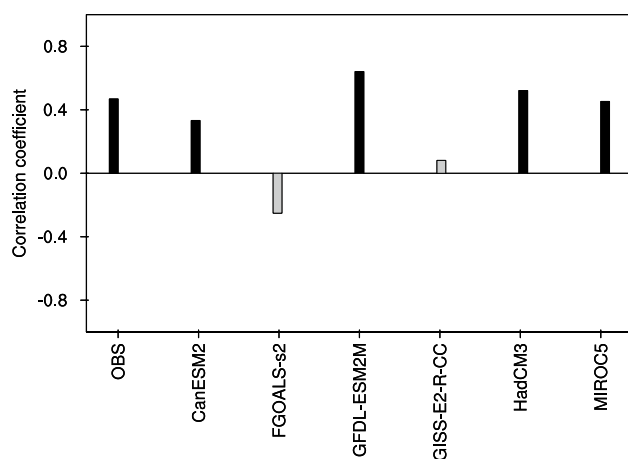


Fig. 5 Correlations between the 21-year running mean NPO indices and the numbers of El Niño Modoki in sliding 21 years. Black (gray) bars indicate the correlation coefficients exceeding (not exceeding) 90% statistical significance level based on a Student's *t* test

NPO leads to a cyclonic circulation located in the subtropical North Pacific. The southwesterly wind anomalies transport warm and wet air into the southeastern quarter of the southern pole of the NPO center, which decrease the surface heat flux from the ocean to atmosphere. The decreasing heat flux induces positive SST anomalies which extend toward the central tropical Pacific and support the development of El Niño Modoki (Yu and Kim 2011).

According to the correlation coefficients between the NPO and the frequency of El Niño Modoki, six models reproducing both the NPO and El Niño Modoki are separated into two groups. One group is called “Good Performance” (GP) in which the models (CanESM2, GFDL-ESM2M, HadCM3, and MIROC5) can simulate the positive relationship between the North Pacific atmospheric circulation and the frequency of El Niño Modoki (Fig. 5). The other is named as “Poor Performance” (PP) in that the models (FGOALS-s2 and GISS-E2-R-CC) fail to capture the observed relationship between the NPO and the frequency of El Niño Modoki.

4.2 Possible cause influencing the NPO-El Niño Modoki simulations

Physical processes responsible for different performances in simulating the relationships between the NPO and the frequency of El Niño Modoki in CMIP5 models are explored. The multi-model ensemble (MME) means of surface wind and SST during boreal spring (March–April–May, MAM) from GP and PP models are calculated, and then a combined EOF (CEOF) analysis is conducted, respectively. The first CEOF modes in the observation and models (not shown) exhibit a horseshoe-like SST pattern and cyclonic circulation

anomalies in the North Pacific poleward of 20°N, which are related to the variations of the Aleutian low (Bond et al. 2003; Di Lorenzo et al. 2008; Ding et al. 2015a, b) and positive SST anomalies in the central-eastern equatorial Pacific. The coupled air-sea interactions are obvious in the central-eastern tropical Pacific. Previous studies suggested that the first leading CEOF mode represents the relationship between the Pacific decadal oscillation (PDO) and the canonical ENSO-related SST (Mantua et al. 1997; Zhang et al. 1997; Ding et al. 2015a, b). The second CEOF mode is usually to illustrate the connections between the NPO and El Niño Modoki via the WES feedback (Yeh et al. 2015). Here, the second CEOF modes in the observation and models are shown in Fig. 6.

From Fig. 6a, the positive phase of the NPO features the anomalous cyclonic and anticyclonic circulations south and north of 45°N in the North Pacific from the observation, and the center of the cyclonic circulation is located around 36.5°N, 150°W. The anomalous southwesterlies generating from the NPO-induced cyclonic circulation in the subtropical Pacific weaken the climatological northeasterly winds, subsequently reduce the upward latent heat flux and lead to sea surface warming. The warm SST anomalies in turn enhance the southwesterly wind, and then extend to the central equatorial Pacific. Such air-sea coupled progress referred to the warm-WES feedback (Xie and Philander 1994) appears clearly in the eastern subtropical North Pacific (green parallelogram box in Fig. 6a). Under the control of the warm-WES feedback, the warm MME mean SST anomalies cover the central equatorial Pacific and the eastern subtropical North Pacific, and then El Niño Modoki tends to develop in the following September–October–November (SON) (Fig. 7a). The spatial pattern of SST and surface wind anomalies closely resembles the Meridional Mode (MM) pattern in the Pacific, with anomalous warm SST and southwesterlies in the vicinity of the Intertropical Convergence Zone (ITCZ) during boreal spring (Chiang and Vimont 2004; Chang et al. 2007, Lin et al. 2015). The MM in the Pacific effectively acts as a conduit through which the extratropical atmosphere influences ENSO (Chang et al. 2007). Lin et al. (2015) also concluded that the MM in the Pacific and its associated subtropical Pacific ocean–atmosphere coupling are important to the generation of El Niño Modoki.

Similar to the observation, the second CEOF mode in the GP models shows the NPO-like pattern with cyclonic and anticyclonic anomalies in the North Pacific south and north of 50°N (Fig. 6b). Coupled with the anomalous southwesterlies and southeasterlies located in the central and northeast subtropical North Pacific, the anomalous warm SST anomalies appear in the subtropical North Pacific. This coupled process extends toward the western and central equatorial Pacific, and induces the westerly anomalies in the western tropical Pacific, which may favor the occurrence of El

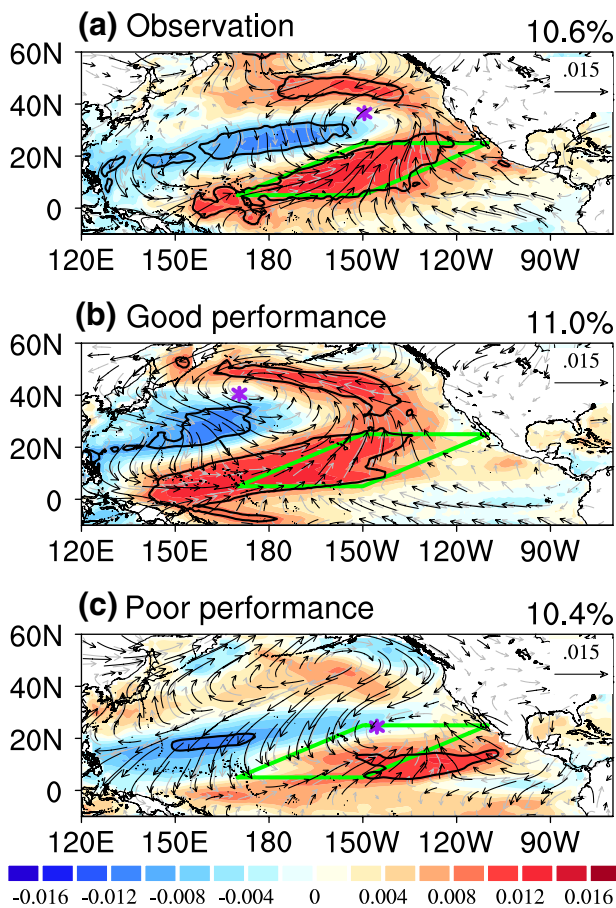


Fig. 6 The second CEOF mode of the observations and MME means of MAM-averaged surface wind (vectors, units: m s^{-1}) and SST anomalies (shaded, $^{\circ}\text{C}$) over the Pacific (10°S – 60°N). **a**, **b** and **c** represent the observation, ensemble mean of GP group models and PP group models, respectively. Bold vectors indicate that the correlations between the wind and PC2 are exceeding the 95% significant level based on a two-tailed Student’s t test. Black contours mean the correlations between the SSTA and PC2 time series exceeding the 95% significance level. The green parallelogram boxes in all plots outlines region where correlations between the SSTA and PC2 time series exceeding the 95% significance level in the observation. The purple asterisks indicate the cyclonic center of each panel

Niño Modoki. It is noted that compared with the observation (Fig. 6a), the cyclonic centers associated with the NPO shift westward to around 170°E , which leads to the westward of the warm-WES feedback centers (Fig. 6b). Due to warm-WES feedback westward shift in GP models, the warm MME mean SST anomalies from the subtropical North Pacific extend to more westward of around 150°E in the tropics during following autumn (Fig. 7b). However, the simulated air-sea coupling processes in the PP models (Fig. 6c) are distinctly different from these in the observation and GP models. Although the NPO pattern in PP models could be reproduced, the south pole center of the NPO (the anomalous cyclonic circulation) locates at about 26.5°N ,

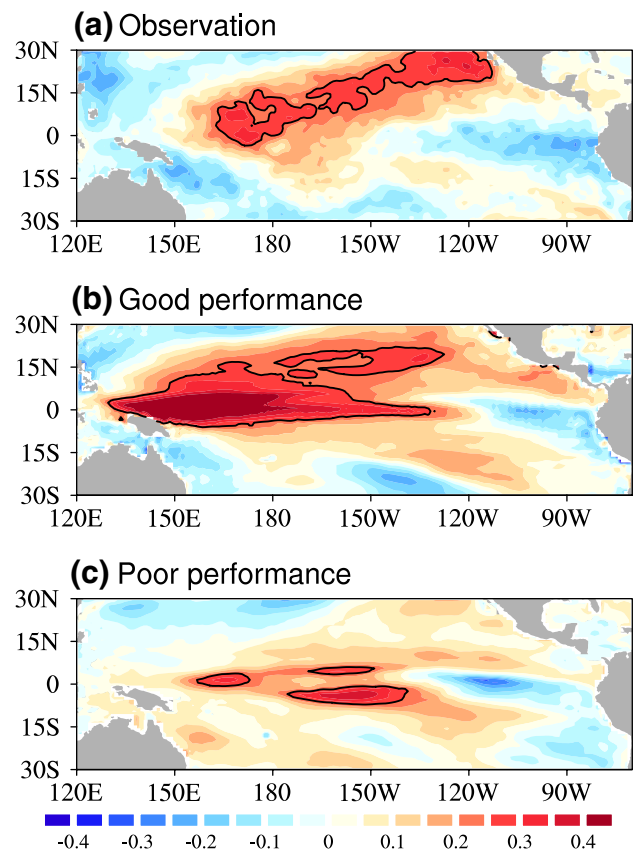


Fig. 7 SSTA patterns during developing autumn (Sept-Oct-Nov) of El Niño Modoki in observation (**a**) and models (**b**, **c**). **a** Is the composited SSTA from observation, while **b** and **c** are the MME mean SSTA from GP group and PP group, respectively. El Niño Modoki event is defined as the value of the PC2 of the DJF-averaged SSTA over the tropical Pacific equal to or greater than 0.7σ . Black contour shown is 0.25°C

145°W , which is southeastward than those in observations and GP models. Therefore, the significant warm-WES feedbacks between the warm SST anomalies and southwesterlies shift in east of 150°W around 10°N . Moreover, the southeastward shift of the anomalous cyclonic circulation of the NPO induces anomalous northerlies in the central subtropical North Pacific (Fig. 6c). The northerly wind anomalies strengthen climatological northeasterly trade wind, and thus lead to cool SST anomalies and northerly anomalies in the western and central subtropical North Pacific and this process is named cool-WES feedback. The cool-WES feedback is unfavorable for the development of the warm SST anomalies in the subtropical North Pacific in the following autumn, and the warm SST anomalies are limited in the central tropical Pacific (Fig. 7c). It is noted that the warm SST anomalies of MME El Niño Modoki in the PP models are much weaker than these in observations and GP models. It is indicated that the failure in simulating the atmospheric-oceanic interactions in the subtropical North Pacific in the PP models

is responsible for the poor performances of relationship between NPO and El Niño Modoki occurrence.

To compare clearly the air-sea interactions in the subtropical North Pacific in observation, GP and PP models, the coupling relationship of SST anomalies and wind anomalies in observation and models are given. Figure 8 shows the scatter diagram of the regressed spring SST and wind speed anomalies in the subtropical North Pacific against with the PC2 of CEOF in observation and each model. The linear slopes in Fig. 8, representing the SST anomaly response to a unit wind speed, can illustrate the intensities of warm-WES feedback in observation and each model. The larger slope means the higher intensities of warm-WES feedback. Given the same wind speed anomalies, the responses of SST anomalies in observation and GP models except for CanESM2 are larger than these in PP models (Fig. 8). Thus, the intensity of air-sea coupling processes in the subtropical North Pacific is suggested to be responsible for the performances of the NPO-El Niño Modoki occurrence relationship in models although the slope for CanESM2 is less smaller than that for FGOALS-s2.

5 Summary and discussion

Previous studies revealed that North Pacific atmosphere variability is connected with El Niño Modoki (Yu et al. 2012a, b; Yeh et al. 2015). However, it is not clear whether climate models can simulate the relationships between the NPO and El Niño Modoki. This study examines the capabilities of 25 CMIP5 models in simulating the relationships between

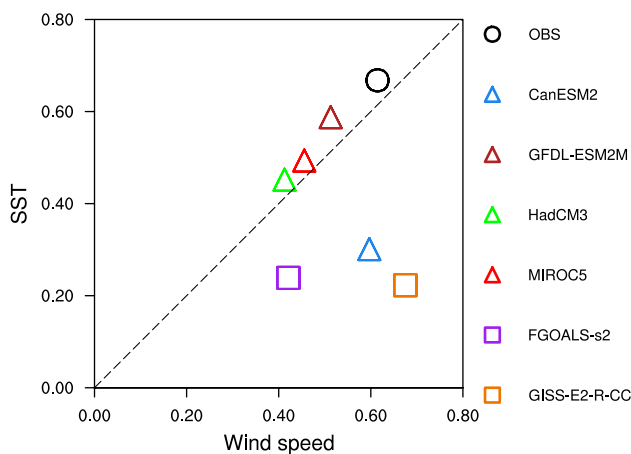


Fig. 8 Scatter diagrams between regressed area-averaged (enclosed area of the green parallelogram box in Fig. 5) SST and wind speed anomalies against the CEOF PC2 in observation and models during boreal spring. The black circle, triangle and square represent the observation, GP and PP models, respectively. The dashed line represents slope equal to value 1. All time series used here are normalized before calculating regression

the North Pacific atmosphere and the frequency of El Niño Modoki, and shows the causes that lead to the discrepancy of simulations among these models.

To evaluate the simulated relationships of the NPO and El Niño Modoki in 25 models, the performances of the models in simulating the NPO and El Niño Modoki are firstly evaluated. All models, except for MRI-CGCM3, can reproduce the NPO pattern. According to different definitions, there are some differences for the identified El Niño Modoki events in the observation and model outputs. Therefore, the two methods are used to define El Niño Modoki in the study. Only six models (CanESM2, FGOALS-s2, GFDL-ESM2M, GISS-E2-R-CC, HadCM3 and MIROC5), in which the El Niño Modoki events identified by the two methods are similar, are used to examine the relationships between the NPO and El Niño Modoki. Compared with the observation, four models (CanESM2, GFDL-ESM2M, HadCM3, and MIROC5) classified as the GP model group can reproduce the positive correlation between the frequency of El Niño Modoki and the NPO, while the other two models (FGOALS-s2 and GISS-E2-R-CC) classified as the PP model group fail to simulate the positive relationship.

According to CEOF analysis, it is suggested that the performances of the positive relationship between the NPO and the frequency of El Niño Modoki in models are associated with the simulated WES feedback process in the eastern subtropical North Pacific. In the GP model group, the MME mean warm SST anomalies are strongly coupled with the southwesterly anomalies in the eastern subtropical North Pacific, and could extend to the central Pacific in the following autumn (Figs. 6b, 7b). In comparison, the coupled warm SST and southwesterly anomalies in the PP model group are rather weak, which may result from the southward shift of the NPO-induced cyclonic circulations (Fig. 6c). Moreover, the performances of the coupled wind-SST relationships in the GP and PP group models are examined individually. The warm WES-feedback intensity in GP group models, except for CanESM2, are similar to the observation, and larger than that in PP models. It indicates that given the same wind speed, the SST anomalies in the eastern subtropical North Pacific in GP group models are warmer than these in PP group models. As for CanESM2, its warm-WES feedback intensity is smaller than that in FGOALS-s2 but larger than that in GISS-E2-R-CC in the PP group models. It is suggested that the relationship between the NPO and the frequency of El Niño Modoki in CanESM2 is influenced by other factor, which is not clear yet.

How El Niño Modoki will change under global warming is still an open question (Yeh et al. 2009; Kim and Yu 2012a; Yu et al. 2017). The results in the present paper suggest that we can analyze the future projection of El Niño Modoki in the multi-model simulations based on the changes of the warm-WES feedback intensity and NPO

in simulations. It is implied that the interactions between the subtropics and tropics should be paid more attentions.

Acknowledgements This work was supported by the CAS/SAFEA International Partnership Program for Creative Research Teams, the Strategic Priority Research Program of the Chinese Academy of Sciences (Grant no. XDA11010403), the National Natural Science Foundation of China (Grant nos. 41422601, 41376025 and 41731173), the Leading Talents of Guangdong Province Program, the Pioneer Hundred Talents Program of the Chinese Academy of Sciences, the National Program on Global Change and Air-Sea Interaction (GASI-IPOVAI-04). SWY was supported by the Korea Meteorological Administration Research and Development Program under grant KMIPA2015-1042.

References

- Anderson BT, Furtado JC, Cobb KM, Di Lorenzo E (2013b) Extratropical forcing of El Niño–Southern Oscillation asymmetry. *Geophys Res Lett* 40:4916–4921
- Ashok K, Behera SK, Rao SA, Weng H, Yamagata T (2007) El Niño Modoki and its possible teleconnection. *J Geophys Res* 112:C11007
- Bond NA, Overland JE, Spillane M, Stabeno P (2003) Recent shifts in the state of the north Pacific. *Geophys Res Lett* 30:2183. <https://doi.org/10.1029/2003GL018597>
- Bretherton CS, Widmann M, Dymnidov VP, Wallace JM, Blade I (1999) The effective number of spatial degrees of freedom of a time-varying field. *J Clim* 12:1990–2009
- Chang P, Zhang L, Saravanan R, Vimont DJ, Chiang JCH, Ji L, Seidel H, Tippet MK (2007) Pacific meridional mode and El Niño–Southern Oscillation. *Geophys Res Lett* 34:L16608. <https://doi.org/10.1029/2007GL030302>
- Chiang J, Vimont D (2004) Analogous Pacific and Atlantic meridional modes of tropical atmosphere–ocean variability. *J Clim* 17:4143–4158
- Deser C, Phillips AS, Tomas RA et al (2012) ENSO and Pacific decadal variability in community climate system model version 4. *J Clim* 25:2622–2651
- Di Lorenzo E, Schneider N, Cobb KM et al (2008) North Pacific Gyre oscillation links ocean climate and ecosystem change. *Geophys Res Lett* 35:L08607
- Di Lorenzo E, Cobb KM, Furtado JC, Schneider N, Anderson BT, Bracco A, Alexander MA, Vimont DJ (2010) Central Pacific El Niño and decadal climate change in the north Pacific Ocean. *Nat Geosci* 3:762–765
- Ding RQ, Li JP, Tseng YH, Sun C, Guo Y (2015a) The Victoria mode in the north Pacific linking extratropical sea level pressure variations to ENSO. *J Geophys Res Atmos* 120:27–45. <https://doi.org/10.1002/2014JD022221>
- Ding RQ, Li JP, Tseng YH (2015b) The impact of south Pacific extratropical forcing on ENSO and comparisons with the north Pacific. *Clim Dyn* 44:2017–2034. <https://doi.org/10.1007/s00382-014-2303-5>
- Ding RQ, Li JP, Tseng YH, Sun C, Zheng F (2016) Linking a sea level pressure anomaly dipole over north America to the central Pacific El Niño. *Clim Dyn*. <https://doi.org/10.1007/s00382-016-3389-8>
- Ding RQ, Li JP, Tseng YH, Sun C, Xie F (2017) Joint impact of north and south Pacific extratropical atmospheric variability on the onset of ENSO events. *J Geophys Res Atmos*. <https://doi.org/10.1002/2016JD025502>
- Furtado JC, Di Lorenzo E, Anderson BT, Schneider N (2012) Linkages between the north Pacific oscillation and central tropical Pacific SSTs at low frequencies. *Clim Dyn* 39:2833–2846
- Ham YG, Kug JS, Park JY, Jin FF (2013) Sea surface temperature in the north tropical Atlantic as a trigger for El Niño/Southern Oscillation events. *Nat Geosci* 6:112–116
- Jin D, Kirtman BP (2009) Why the southern hemisphere ENSO responses lead ENSO? *J Geophys Res* 114:D23101. <https://doi.org/10.1029/2009JD012657>
- Kalnay E, Kanamitsu M, Kistler R et al (1996) The NCEP/NCAR 40-year reanalysis project. *Bull Am Meteorol Soc* 77:437–471
- Kao HY, Yu JY (2009) Contrasting eastern-Pacific and central-Pacific types of ENSO. *J Clim* 22:615–632
- Kim ST, Yu JY (2012) The two types of ENSO in CMIP5 models. *Geophys Res Lett* 39:L11704. <https://doi.org/10.1029/2012GL052006>
- Kim HM, Webster PJ, Curry JA (2009) Impact of shifting patterns of Pacific Ocean warming on north Atlantic tropical cyclones. *Science* 325:77–80
- Kug JS, Jin FF, An SI (2009) Two types of El Niño events: cold tongue El Niño and warm pool El Niño. *J Clim* 22:1499–1515
- Larkin NK, Harrison DE (2005) Global seasonal temperature and precipitation anomalies during El Niño autumn and winter. *Geophys Res Lett* 32:L16705
- Lin CY, Yu JY, Hsu HH (2015) CMIP5 model simulations of the Pacific meridional mode and its connection to the two types of ENSO. *Int J Climatol* 35:2352–2358. <https://doi.org/10.1002/joc.4130>
- Ma J, Yu JY (2014) Linking centennial surface warming patterns in the equatorial Pacific to the relative strengths of the Walker and Hadley circulations. *J Atmos Sci* 71:3454–3464
- Ma J, Xie SP, Xu H (2017) Contributions of the North Pacific meridional mode to ensemble spread of ENSO prediction. *J Clim* 30(22):9167–9181
- Mantua NJ, Hare SR, Zhang Y, Wallace JM, Francis RC (1997) A Pacific interdecadal climate oscillation with impacts on salmon production. *Bull Am Meteorol Soc* 78:1069–1079
- Mo KC (2010) Interdecadal modulation of the impact of ENSO on precipitation and temperature over the United States. *J Clim* 23:3639–3656
- Park JY, Yeh SW, Kug JS, Yoon J (2013) Favorable connections between seasonal footprinting mechanism and El Niño. *Clim Dyn* 40:1169–1181
- Rayner NA, Parker DE, Horton EB et al (2003) Global analyses of sea surface temperature, sea ice, and night marine air temperature since the late nineteenth century. *J Geophys Res* 108:4407. <https://doi.org/10.1029/2002JD002670>
- Ren HL, Jin FF (2011) Niño indices for two types of ENSO. *Geophys Res Lett* 38:L04704. <https://doi.org/10.1029/2010GL046031>
- Rogers JC (1981) The north Pacific oscillation. *J Climatol* 1(1):39–57
- Tan W, Wang X, Wang WQ, Wang CZ, Zuo JC (2016) Different responses of sea surface temperature in the south China Sea to various El Niño events during boreal autumn. *J Clim* 29:1127–1142
- Taschetto AS, England MH (2009) El Niño Modoki impacts on Australian rainfall. *J Clim* 22:3167–3174
- Taschetto AS, Gupta AS, Jourdain NC, Santoso A, Ummenhofer CC, England MH (2014) Cold tongue and warm pool ENSO events in CMIP5: mean state and future projections. *J Clim* 27:2861–2885
- Vimont DJ, Battisti DS, Hirst AC (2001) Footprinting: a seasonal connection between the tropics and mid-latitudes. *Geophys Res Lett* 28:3923–3926. <https://doi.org/10.1029/2001GL013435>
- Vimont DJ, Wallace JM, Battisti DS (2003a) The seasonal footprinting mechanism in the Pacific: implications for ENSO. *J Clim* 16:2668–2675
- Vimont DJ, Battisti DS, Hirst AC (2003b) The seasonal footprinting mechanism in the CSIRO general circulation models. *J Clim* 16:2653–2667

- Walker GT, Bliss EW (1932) World weather V. *Mem Roy Meteor Soc* 4:53–84
- Wang CZ, Wang X (2013) Classifying El Niño Modoki I and II by different impacts on rainfall in Southern China and typhoon tracks. *J Clim* 26:1322–1338
- Wang X, Wang CZ (2014) Different impacts of various El Niño events on the Indian Ocean dipole. *Clim Dyn* 42:991–1005
- Wang X, Zhou W, Li C, Wang D (2014) Comparison of the impact of two types of El Niño on tropical cyclone genesis over the south China Sea. *Int J Climatol* 34:2651–2660. <https://doi.org/10.1002/joc.3865>
- Wang CZ, Deser C, Yu JY, Di Nezio P, Clement A (2016) El Niño–Southern Oscillation (ENSO): a review. In: Glynn P, Manzello D, Enochs I (eds) *Coral reefs of the eastern Pacific*. Springer, Berlin, pp 85–106
- Weng H, Ashok K, Behera SK, Rao SA (2007) Impacts of recent El Niño Modoki on dry/wet conditions in the Pacific rim during boreal summer. *Clim Dyn* 29:113–129
- Xie SP, Philander SGH (1994) A coupled ocean–atmosphere model of relevance to the ITCZ in the eastern Pacific. *Tellus* 46A:340–350
- Xu K, Tam C, Zhu C, Liu B, Wang W (2016) CMIP5 Projections of two types of El Niño and their related tropical precipitation in the 21st century. *J Clim*. <https://doi.org/10.1175/JCLI-D-16-0413.1>
- Yeh SW, Kug JS, Dewitte B, Kwon MH, Kirtman BP, Jin FF (2009) El Niño in a changing climate. *Nature* 461:511–514. <https://doi.org/10.1038/nature08316>
- Yeh SW, Wang X, Wang CZ, Dewitte B (2015) On the relationship between the north Pacific climate variability and the central Pacific El Niño. *J Clim* 28:663–677. <https://doi.org/10.1175/JCLI-D-14-00137.1>
- Yu JY, Kao HY (2007) Decadal changes of ENSO persistence barrier in SST and ocean heat content indices: 1958–2001. *J Geophys Res* 112:D13106
- Yu JY, Kim ST (2010) Identification of central-Pacific and eastern-Pacific types of ENSO in CMIP3 models. *Geophys Res Lett* 37(15):L15705
- Yu JY, Kim ST (2011) Relationships between extratropical sea level pressure variations and the central Pacific and eastern Pacific types of ENSO. *J Clim* 24:708–720. <https://doi.org/10.1175/2010JCLI3688.1>
- Yu JY, Kim ST (2013) Identifying the types of major El Niño events since 1870. *Int J Climatol* 33(8):2105–2112
- Yu JY, Kao HY, Lee T (2010) Subtropical-related interannual sea surface temperature variability in the central equatorial Pacific. *J Clim* 23:2869–2884. <https://doi.org/10.1175/2010JCLI3171.1>
- Yu JY, Lu MM, Kim ST (2012a) A change in the relationship between tropical central Pacific SST variability and the extratropical atmosphere around 1990. *Environ Res Lett* 7:034025. <https://doi.org/10.1088/1748-9326/7/3/034025>
- Yu JY, Zou Y, Kim ST, Lee T (2012b) The changing impact of El Niño on US winter temperatures. *Geophys Res Lett* 39:L15702. <https://doi.org/10.1029/2012GL052483>
- Yu JY, Wang X, Yang S, Paek H, Chen MY (2017) Changing El Niño–southern oscillation and associated climate extremes. Book chapter in *climate extremes: patterns and mechanisms*. In: Wang S-Y, Jin-Ho Y, Chris F, Gillies RR (eds) *AGU geophysical monograph series*, vol 226, pp 3–38. AGU, Washington, DC
- Yuan Y, Yang S (2012) Impacts of different types of El Niño on east Asian climate: focus on ENSO cycles. *J Clim* 25:7702–7722
- Zhang Y, Wallace JM, Battisti DS (1997) ENSO-like interdecadal variability. *J Clim* 10:1004–1020